Pre-annealing treatment effects on the electrochemical performances of lithium-rich layered oxide cathodes for Li-ion battery

4 authors:

Samuel Ajayi
Covenant University Ota Ogun State, Nigeria
24 PUBLICATIONS   **188** CITATIONS

SEE PROFILE

Cyril Ehi-Eromosele
Covenant University Ota Ogun State, Nigeria
71 PUBLICATIONS   **666** CITATIONS

SEE PROFILE

Ajanaku Kolawole Oluseyi
Covenant University Ota Ogun State, Nigeria
81 PUBLICATIONS   **964** CITATIONS

SEE PROFILE

Joseph Adekoya
Covenant University Ota Ogun State, Nigeria
44 PUBLICATIONS   **336** CITATIONS

SEE PROFILE

Some of the authors of this publication are also working on these related projects:

Project   Assessment of the Levels of Pesticide Residues Present in Soil Samples from Wazo Market, Ogbomoso, Nigeria. View project

Project   Development of Hybrid Organic Coatings from Seed oils View project

Pre-annealing treatment effects on the electrochemical performances of lithium-rich layered oxide cathodes for Li-ion battery

Samuel O. Ajayi[1], Cyril O. Ehi-Eromosele[1,*] (iD), Kolawole O. Ajanaku[1], and Joseph A. Adekoya[1]

[1] *Department of Chemistry, Covenant University, PMB 1023, Ota, Nigeria*

ABSTRACT

Lithium-rich layered oxides (LLOs) are highly promising cathodes for high-capacity Li-ion batteries (LIBs). Typically, high annealing temperatures and durations have been used in the synthesis of these materials. Appropriate synthetic methods must be employed to successfully synthesise them at lower annealing temperatures. Herein, the effects of pre-annealing temperature on the structural and electrochemical performances of the LLOs are evaluated. X-ray diffraction and Raman spectra analysis show that the pre-annealed samples displayed higher crystal defects such as dislocation density, micro-strain, cationic disorder and smaller crystallites compared to the post-annealed sample. Also, the pre-annealed cathode materials showed better electrochemical performances, including higher specific capacity, excellent rate performance, and better cycling stability. The much improved electrochemical performances of the pre-annealed cathodes were explained on the basis of their higher crystal defects which reduce the energy barrier for lithium-ion mobility. In addition, pre-annealing allowed the synthesis of these LLOs at a lower temperature and annealing duration which could help reduce the cost of LIBs. These results show that pre-annealing treatment is also an important synthesis parameter that could be exploited to optimise the structure–function relationships in materials to achieve optimal performance.

1 Introduction

The structure and electrochemical performance of the LLOs depend on their compositions, i.e. the Li and transition metal ratio [1]. The structural and electrochemical performances of LLOs have been improved by surface modification [2, 3], lattice doping [4, 5], core–shell architecture [6, 7], nanostructuring [8], doping of a spinel structure [9, 10] and optimisation of the synthetic methods [11–13]. In addition, various synthetic methods have been used to influence the structure and electrochemical performance of these

materials. Depending on the method of synthesis, several synthesis parameters can be used to influence the product characteristics such as morphology, cation mixing, crystallinity, and so on. Thermal annealing (so-called post-annealing treatment) is one of the main synthesis conditions that have been used to modulate the structure–property relations of ceramic oxides including LLOs. For example, Li_2MnO_3 positive electrode material synthesised with low temperature treatments (400–600 °C) has been shown to have better electrochemical performance than the analogues treated with higher temperature, even though it displays very poor cycle performance and voltage dropping issues [14, 15]. Also, Vu et al. reported the effect of annealing temperature on the phase components, cation disorder, crystal defects and electrochemical performance of an integrated spinel-LLO cathode material [10].

In most of the reports on the synthesis of LLOs, high annealing temperature (800–1200 °C) and annealing duration (8–20 h) are usually required to obtain a highly crystalline material [6, 7, 10–12]. In our previous study [12], it was established that the optimal post-annealing temperature that produced the highest crystallinity and electrochemical performance for the studied LLO cathodes ($Li_{1.2}Mn_{0.52}Ni_{0.20}Co_{0.08}O_2$) was 1000 °C for 10 h. Nomura et al. [11] also reported that an optimal post-annealing temperature of 1000 °C for 12 h produced LLO cathodes ($Li_{1.2}Ni_{0.18}Co_{0.03}Mn_{0.58}O_2$) with the best electrochemical performance. Furthermore, many reports [3–5, 13–15] have incorporated pre-annealing and post-annealing treatments in the synthesis of LLO cathode materials. In many of these reports, the post-annealing temperature and duration of annealing is reduced after the pre-annealing step compared with the studies that uses only the post-annealing treatment of LLO cathode materials. Pre-annealing of ceramic oxides which is normally done at a much lower temperature than post-annealing treatment has been used firstly to remove precursor organic materials and can also modulate the microstructure of the final product.

Studies of the effects of pre-annealing temperature on the structure and electrochemical properties of LLO cathode material are very scarce. Applying pre-annealing treatment during synthesis of LLO is expected to change their structure and cathode performance. Therefore, $Li_{1.2}Mn_{0.52}Ni_{0.20}Co_{0.08}O_2$ cathodes were synthesised using sol–gel combustion

method to establish the relationship between the pre-annealing temperature of these LLOs with their structural and electrochemical performances. Cathode samples that were pre- and post- annealed were compared with one that was only post-annealed on the basis of the changes observed in their structural and electrochemical properties. It is important to state that a detailed study on the effects of fuel types and annealing temperature on the combustion synthesis of these cathode materials has already been reported elsewhere [16]. Pre-annealing allowed the post-annealing treatment of the samples to be done at a much lower temperature and duration thereby saving energy.

2 Experimental

2.1 Synthesis

All chemicals were of Analar grade and were used as received. The $Li_{1.2}Mn_{0.52}Ni_{0.20}Co_{0.08}O_2$ cathode materials were prepared by the citric acid-ammonium acetate mediated sol–gel combustion synthesis as already reported [16]. In a typical procedure, lithium nitrate ($LiNO_3$, 0.83 g), manganese (II) nitrate tetrahydrate ($Mn(NO_3)_2 \cdot 4H_2O$, 1.31 g), nickel (II) nitrate hexahydrate ($Ni(NO_3)_2 \cdot 6H_2O$, 0.58 g), cobalt (II) nitrate hexahydrate ($Co(NO_3)_2 \cdot 6H_2O$, 0.23 g), citric acid monohydrate ($C_6H_8O_7 \cdot H_2O$, 1.24 g) and ammonium acetate ($C_2H_7NO_2$ 0.25 g) were dissolved in 20 ml of distilled water and the solutions were heated to 80 °C under magnetic stirring to form a viscous gel of precursors. The gel was heated at 300 °C resulting in swelling, evolution of gases and ignition. The product formed was grounded and divided into three portions with each portion thermally treated in a muffle furnace, at a rate of 2 °C min^{-1} to obtain the final product. The first portion was annealed at 1000 °C for 10 h, grounded and named T1 sample. The other portions were pre-annealed at 500 °C for 3 h before annealing one at 1000 °C for another 3 h (denoted T2 sample), while the other one was annealed at 900 °C for 3 h (denoted T3 sample).

2.2 Characterisation of synthesised cathode materials

Powder X-ray diffraction (XRD) measurements were done using a STOE STADI MP diffractometer with MoKα radiation ($\lambda = 0.709320$ Å) and a MYTHEN 1 K detector. The diffractions patterns were obtained using 2θ range of 3°–50° at a step width of 0.015°. Raman spectra of the sample powders were obtained using Raman spectrometer (Horiba LabRam HR Evolution) with a 632 nm laser.

2.3 Electrochemical characterisation

The positive electrode was made by mixing the synthesised LLO powders, carbon black, and polyvinylidene fluoride binder with mass ratio of 80:10:10, respectively. The resulting slurry was deposited on an Al foil using a doctor-blade coater (150 μm gap) and dried at 80 °C overnight in a vacuum oven. The mass loading of the active materials was about 3.8 mg cm^{-2}. The electrochemical characterisations of the samples were performed using a CR2032 coin cell, fabricated inside the glovebox filled with argon, using the positive material already prepared as cathode, lithium metal as anode and porous Celgard 2325 as the separator. The electrolyte (LP30 selectylite, BASF) consists of 1 M lithium hexafluorophosphate (LiPF$_6$) in 1:1 (v/v) ethylene carbonate/dimethyl carbonate. Galvanostatic charge/discharge tests were performed between 2.0 and 4.8 V (vs Li/Li$^+$) at 25 °C with different current densities. Electrochemical impedance spectroscopy (EIS) analysis was undertaken in the frequency range of 1 Hz–1 MHz. A VMP3 multi-channel potentiostat (Biologic) was used for all the electrochemical measurements.

3 Results and discussion

3.1 XRD analysis

The structural properties of the T1, T2 and T3 powder samples were determined from the X-ray diffraction analysis. Figure 1 gives the XRD patterns of the samples annealed at different temperatures. The XRD patterns can be attributed to the monoclinic layered system with space group of C2/m and they all gave sharp peaks with no visible secondary phase. Also,

all the samples displayed well crystalline layered structures as seen from the clear splitting of the 13-3 and 33-1 peaks. The peak reflections observed between 9° and 13° in Fig. 1 can be attributed to the stacking sequence of C2/m.

Table 1 gives the other structural properties of the samples which were obtained from the Rietveld refinement of the XRD data as already reported in our previous communication [16]. It can be seen that the T1 sample showed the highest lattice parameter values and the T3 sample gave the least of these properties. The T1 sample gave a, b and c lattice constants of 4.955, 8.571 and 5.037 Å while the T3 sample gave 4.937, 8.547 and 5.025 Å, respectively. Correspondingly, the T1 sample had the largest unit cell volume (213.92 Å^3) while the T3 sample gave the least (212.04 Å^3). It is observed that the full-width-at-half-maximum (FWHM) of the T1 sample is the smallest (0.0762°) while that of the T3 sample is the highest (0.0801°) showing the decreased crystallinity of the T3 sample which was pre-annealed and post-annealed at a lesser temperature and duration compared to the T1 sample which was only post-annealed at a higher temperature and longer duration. The T1 samples showed the highest crystallite size (48.16 nm) while the T3 sample gave the least (45.80 nm). It is well known that the crystallinity and crystallite size of ceramics increases with temperature increase. The direct influence of particle size on lattice parameters and unit cell volume is also noticed from XRD analysis. The particle size increases with increase in the values of lattice parameters and unit cell volume as shown in Table 2. Furthermore, the T3
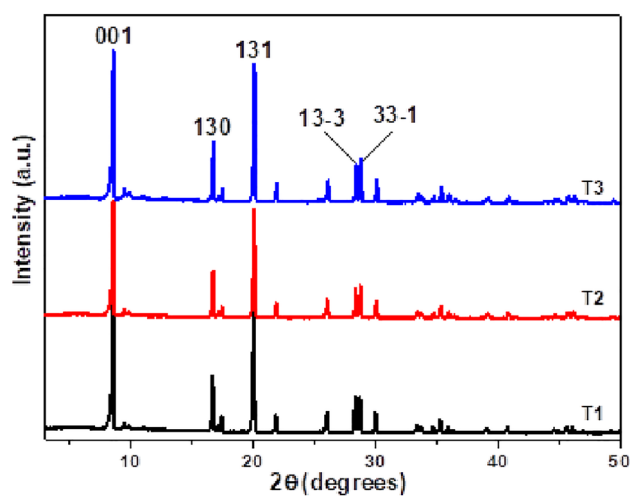

Fig. 1 XRD patterns of LLO samples

Table 1 Structural properties of the LLO powders

Sample	T1	T2	T3
Space group	C2/m	C2/m	C2/m
a (Å)	4.955	4.944	4.937
b (Å)	8.571	8.558	8.547
c (Å)	5.037	5.030	5.025
V (Å^3)	213.918	212.823	212.038
FWHM (001) peak (°)	0.0762	0.0788	0.0801
Crystallite size, D (nm)	48.16	46.56	45.80
Dislocation density, $\delta \times 10^{-3}$ (nm^{-2})	0.43	0.46	0.48
Micro-strain, $\varepsilon \times 10^{-3}$	255.32	264.03	267.92
Peak intensity ratio, I_{001}/I_{131}	1.15	1.09	1.10

sample gave higher dislocation density and lattice strain values compared to the T1 sample which gave the least values. Dislocation density and other lattice imperfections usually cause diffraction line broadening that leads to lattice strain [17]. In addition, T1 sample gave the highest peak intensity ratio (I_{001}/I_{131}) while the T2 and T3 samples gave lesser I_{001}/I_{131} indicating higher cationic disorder in the pre-annealed samples. Generally, I_{001}/I_{131} values can be used to indicate the extent of cation mixing in transition metal (TM) oxides with comparatively higher I_{001}/I_{131} values showing lesser cation mixing [18]. Usually in Li–Mn–Ni–Co–O system, good cation ordering between the Li sublattice and TM sublattice increases with higher synthesis temperature. The XRD analysis results show that applying lesser temperature annealing conditions (seen in the pre-annealed samples) leads to higher lattice imperfections such as increase in dislocations, cationic disorder and crystallite smallness which are the main contributors to lattice strain. Similar results from XRD analysis showing several lattice imperfections associated with poor crystallinity and low annealing temperatures have been reported elsewhere [10, 17, 19]. The structural parameters are calculated from the following equations,

$$D = \frac{k\lambda}{\beta \mathrm{Cos}\theta} \tag{1}$$

$$\delta = \frac{1}{D^2} \tag{2}$$

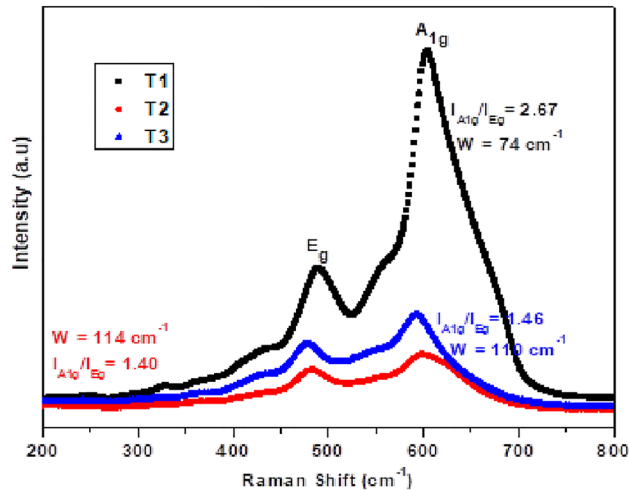$$\varepsilon = \frac{\beta}{4\mathrm{Tan}\theta} \tag{3}$$

where D is the crystallite size, λ is wavelength of X-ray, θ is Braggs angle, β is FWHM, δ is the dislocation density, and ε is the micro-strain.

3.2 Raman analysis

Figure 2 gives the Raman spectra of the LLO powder samples. Raman spectra analysis can be used to correlate the microstructural parameters obtained from XRD analysis. The Raman spectra peaks of all samples can be assigned to the typical vibration modes of the LLO [12]. All the Raman spectra give the characteristic two main peaks seen in the Raman spectra of LLO namely, the A_{1g} and E_g corresponding to the stretching and bending modes of TM–O bonds, respectively. It has been shown that the crystallite size of nanomaterials has an inverse relationship with the Raman peak broadening (W) value [16, 20]. As can be seen from Fig. 2, the A_{1g} peak broadening

Table 2 Electrochemical data from the first cycle charge/discharge capacity of the LLO cathodes

Sample	Charge capacity (mAh g^{-1})	Discharge capacity (mAh g^{-1})	IRC loss (mAh g^{-1})	Coulombic efficiency (%)	Capacity retention after 30 cycles (%)
T1	268	151	117	56	118
T2	304	179	125	59	122
T3	274	179	96	65	111

Fig. 2 Raman spectra of the LLO samples

($W = 74$ cm^{-1}) of the T1 sample is the least compared to the T2 and T3 samples which displayed comparable higher W values. As a result, the T1 sample gave the highest crystallite size while the T2 and T3 samples had comparable smaller crystallite sizes, confirming the results obtained from the XRD analysis as shown in Table 1. The T1 sample showed much higher peaks than the pre-annealed samples which confirms its better crystallinity. Furthermore, the absolute intensity ratio of the two main Raman peaks (I_{A1g}/I_{Eg}) has been used to indicate cationic mixing in the TM layer, where a higher I_{A1g}/I_{Eg} value implies a lesser cationic disorder [16, 20]. The T1 sample presented the highest $I_{A1g}/I_{Eg} = 2.67$ while the pre-annealed T2 and T3 samples gave 1.40 and 1.46, respectively. Also, like in the I_{001}/I_{131} analysis of the XRD, the T1 sample had the least cationic mixing compared to the pre-annealed samples. The Raman spectroscopy results confirms the XRD results and also show that pre-annealing conferred lattice imperfections on the LLO crystallite which can be traced to their poorer crystallinity compared to the T1 samples.

3.3 Electrochemical performances of LLO cathodes in Li-ion battery

The initial cycle charge–discharge profiles, cycling performances and the Coulombic efficiencies of the T1, T2 and T3 cathodes cycled between 2.0 and 4.8 V using a current rate of 10 mA/g (0.05C, where 1C = 200 mA/g) are depicted in Fig. 3a–c, respectively. Some of these galvanostatic cycling results of

the cathode materials have also been reported in our previous communication [16]. Relevant electrochemical data obtained from the initial charge–discharge profiles of the cathodes are shown in Table 2. Figure 3a shows that all the cathodes show the distinctive profiles of LLOs during the initial charge which consists of two regions. The two regions are the sloping region (i.e. open circuit voltage to $\sim$ 4.5 V) indicating Li$^+$ extraction from material, and a plateau region (4.5–4.8 V) corresponding to the extraction of Li$^+$ leading to the irreversible loss of Li$_2$O. The initial charge capacity of T1, T2 and T3 cathodes is 268, 304, and 274 mAh/g, while their corresponding discharge capacity is 151, 179 and 179 mAh/g, respectively. The pre-annealed samples (T2 and T3) gave higher initial discharge capacities than the post-annealed sample (T1). Also, Table 2 shows that the first cycle irreversible capacity loss (IRC) of TI, T2 and T3 cathodes is 117, 125 and 96 mAh/g, respectively.

In Fig. 3b, all the cathodes display increasing discharge capacity with cycling as shown in their capacity retention values after 30 cycles which is over 100% (Table 2). The increasing discharge capacity after several cycles suggest gradual activation of the synthesised materials which in turn improved their cycling stability [16, 20]. However, the cathodes made from the pre-annealed powders (T2 and T3) gave higher discharge capacities than the cathode made from the post-annealed T1 sample. Particularly, the T2 cathode gave an initial discharge capacity of 179 mAh/g and 218 mAh/g after 30 cycles while the T1 cathode gave an initial discharge capacity of 151 mAh/g and 178 mAh/g after 30 cycles. Even though the initial capacities of the cathodes were low, their capacities increased with cycling. Usually, LLOs generally experience gradual drop in their operating voltage during extended cycling which causes a concomitant drop in their capacity with cycling. The Coulombic efficiency (CE) of the cathodes is shown in Fig. 3c. The first cycle CE of T1, T2 and T3 cathodes is 56, 59, and 65%, respectively (Table 2). On subsequent cycling to the 30th cycle, the CE increased with the T1 steadying about 100%, the T2 was above 100% while the T3 was generally below 100%. The capacity retention of the cathodes after 30 cycles exceeds 100% (Table 2). This could be due to the slow activation of these materials and their low initial discharge capacity since capacity retention is a function of the initial discharge capacity. These results show that the pre-annealed cathodes (T2 and T3) gave better
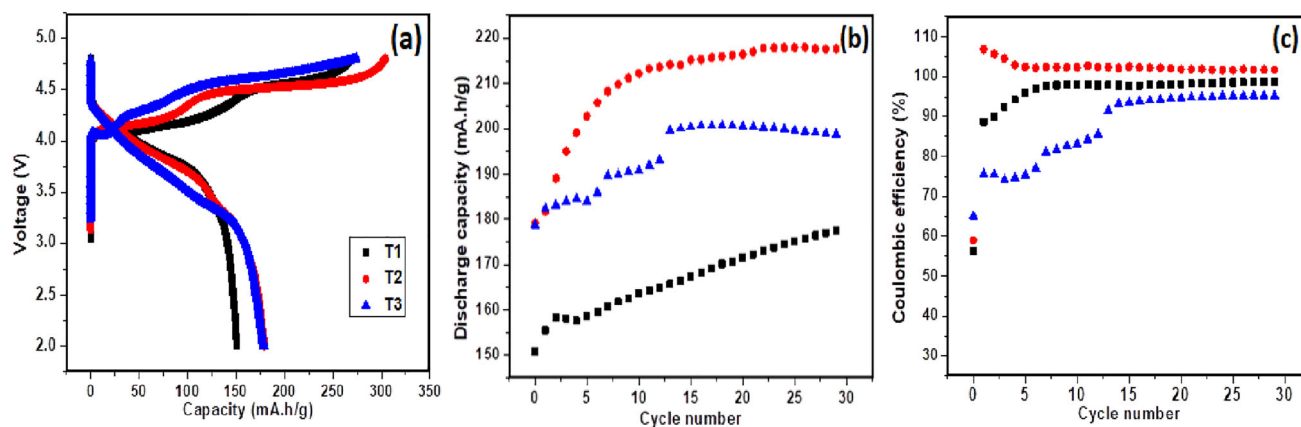
Fig. 3 a First cycle charge–discharge curves, **b** cycle performance, and **c** Coulombic efficiency. The cathodes vs Li$^+$/Li where cycled between 2.0 and 4.8 V using a current rate of 10 mA g^{-1} at 25 °C

cycling performance than the post-annealed cathode (T3). The initial CE and cycling stability obtained in this study are comparable to the reported data on LLO materials. [4, 15, 21, 25–27].

To further evaluate the influence of the LLO structures on their electrochemical performance, the rate performance of the LLO cathodes was undertaken. Figure 4a shows the rate performance of the LLO cathodes cycled at different current densities (10–200 mA/g or 0.05C-1C) between 2.0 and 4.8 V. The discharge capacities of all cathodes gradually reduce as the current density increases. This could be attributed to reduction in time for intercalation of Li$^+$ into the crystal lattice and increase in polarisation as the current density increases [15]. All the cathodes displayed good reversible capacity, after high rate cycling, as they maintained similar and stable discharge capacities when the current density was switched back to 10 mA/g. Nevertheless, the pre-annealed cathodes (T2 and T3) displayed a much more superior rate performance compared to the post-annealed cathode (T1). Particularly, the T3 cathode had the highest discharge capacities at all current densities. Unlike with the other cathodes, the discharge capacity observed in the rate performance test at 10 mA/g (0.05 C) for T3 material was surprisingly higher than those observed from galvanostatic cycling.

The cycling and rate performances of these LLO cathodes can be explained on the basis of their lattice imperfections as indicated by their cationic disorder and crystallite sizes, for example. LLO materials with good cationic ordering are usually desired for better electrochemical performance. Though

inevitable during the synthesis and cycling of the LLOs, Li/Ni intermixing in both the TM and Li layers has been shown to affect the rate capability of these materials since it can limit Li mobility [21]. However, cation-disordered cathode materials have been shown to be beneficial to the electrochemical performance of lithium-ion batteries since they can promote the formation of smooth Li transport by percolation and also facilitate the extraction of labile oxygen electrons which can contribute to the capacity [10, 22]. Furthermore, the outstanding rate performance and excellent recovery capability of the T3 cathode can be attributed to its crystallite size which was the smallest compared to the other LLO materials. It is well known that small crystallites can increase the kinetics of Li$^+$ intercalation and lower the charge transfer resistance during electrochemical cycling, thereby improving rate performance [20, 23]. It has been shown, in the XRD and Raman spectra analysis, that the pre-annealed LLO materials (mostly the T3) with higher lattice imperfections presented better electrochemical performance than the T1 cathode with lesser crystalline defects.

Figure 4b–d gives the electrochemical impedance spectroscopy (EIS) of the cathodes which were measured prior to galvanostatic cycling. The Nyquist plots for the T1, T2 and T3 cathodes are shown in Fig. 4b and the inset diagram shows the enlargement of the semi-circle in the high-frequency region. The equivalent circuit model used for fitting the EIS data and the obtained parameters are given in Fig. 4c and d, respectively. The Nyquist plots consist of compressed semicircles in high-frequency region and the linear portion (long tail) in the low-frequency region,
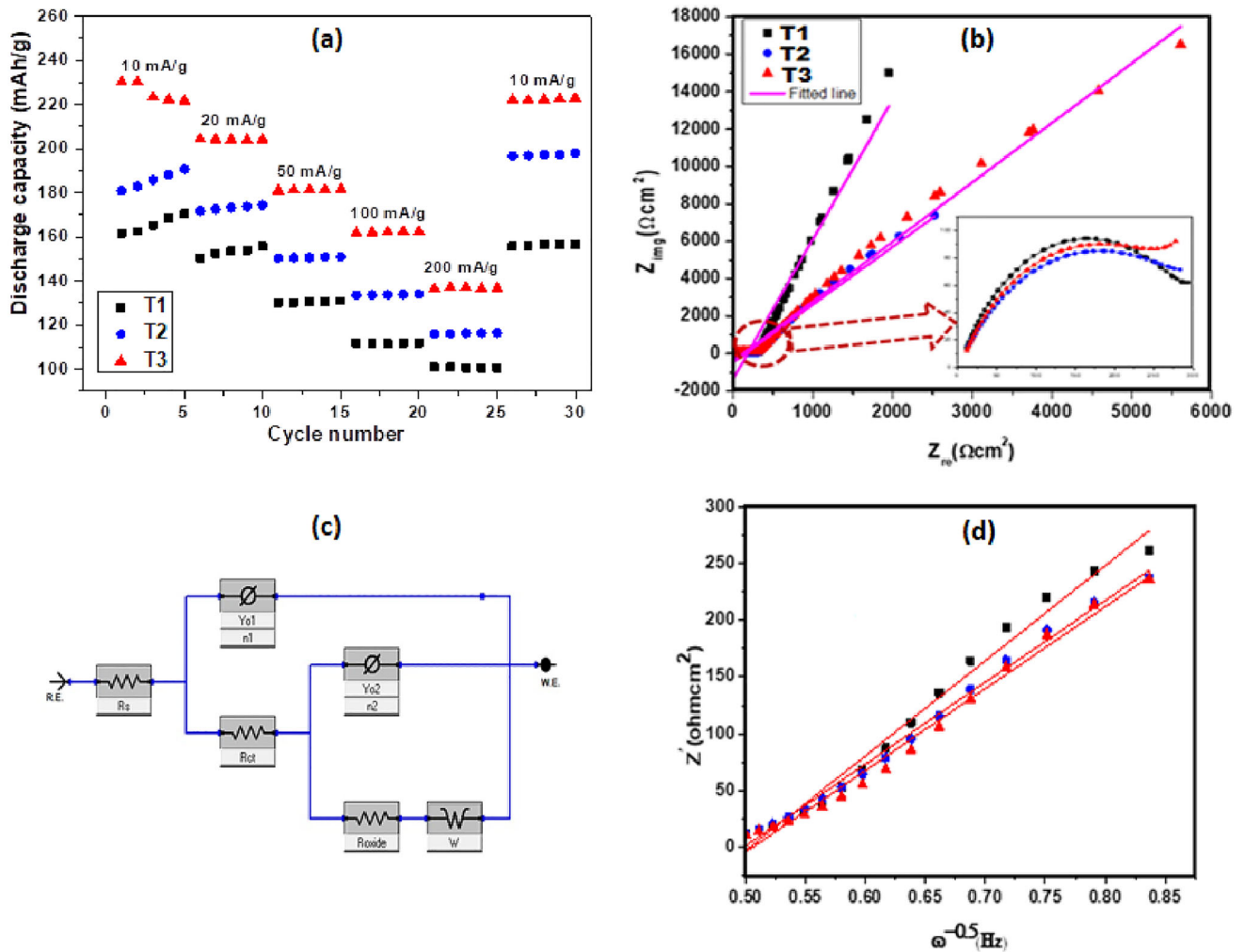
Fig. 4 a Rate capability (**b**) Nyquist plots (**c**) Equivalent circuit model (**d**) Plots of Z′ vs $\omega^{-0.5}$ of LLO cathodes (vs Li$^+$/Li)

which is due to the resistance from surface film, charge transfer resistance (R_{ct}) and lithium-ion diffusion in electrode, respectively [24]. The T1 cathode displays the highest R_{ct} while the T3 cathode shows the least, which indicates the fast electrode reaction kinetics of the T3 cathode. The lithium-ion diffusion coefficient (D) of the cathodes is calculated from the low-frequency line according to Eqs. (4) and (5):

$$D = 0.5\left(\frac{RT}{AF^2\delta_w C}\right)^2 \tag{4}$$

$$Z = R_s + R_{ct} + \delta_w \cdot \omega^{-0.5} \tag{5}$$

where R is the gas constant, T is the absolute temperature, A is the surface area of the electrode, F is the Faraday constant, C is the molar concentration of lithium ions in active material, R_s is the solution resistance, and δ_w is the Warburg factor determined

by Z and $\omega^{-0.5}$. The linear relationship between Z and $\omega^{-0.5}$ in the low-frequency region is shown in Fig. 4d, with which the Warburg factor, δ_w, can be derived [24]. The current density (i_o) is calculated using Eq. (6) where n represents the number of transferred electrons.

$$i_o = \frac{RT}{nAF^2\delta_w C} \tag{6}$$

The lithium-ion diffusion coefficient (D) of the pre-annealed samples ($\sim 4.75 \times 10^{-20}$ cm^2 s^{-1} for both the T2 and T3 cathodes) are higher than the post-annealed sample (3.43×10^{-20} cm^2 s^{-1} for T1 cathode), showing the effect of pre-annealing on the lithium-ion diffusion in the active particles (Table 3). The EIS results show that the T1 cathode had the highest $R_{ct\ and}\ \delta_w$ and the lowest D and i_o values compared to the T2 and T3 cathodes. These negative

Table 3 EIS parameters of the LLO cathodes

Cathode	R_s (Ω cm^2)	R_{ct} (Ω cm^2)	δ_w (Ω cm^2)	D (cm^2 s^{-1}) $\times 10^{-20}$	i_o (μAcm^{-2})
T1	2.40	95,000	836.10	3.43	0.013
T2	4.30	71,500	719.52	4.75	0.355
T3	0.93	35,900	719.98	4.74	0.707

EIS parameters for the T1 cathode were detrimental to its electrochemical performance. The better electrochemical performance of the pre-annealed T2 and T3 cathodes could be attributed to their lattice imperfections which reduced the energy barrier and aided faster lithium-ion diffusion in these materials.

4 Conclusions

The effect of pre-annealing temperature on the structure and electrochemical properties of LLO cathode materials have been studied. Pre-annealing allowed for post-annealing at a shorter temperature and duration which was shown to reduce lithium loss and avoid the usual practice of adding excess lithium during synthesis of electrode materials, thereby can help reduce the cost of Li-ion batteries. The study showed that pre-annealing induced higher lattice imperfections such as increase in dislocations, cationic disorder and crystallite smallness which particularly improved the electrochemical performance of the cathode materials.Q The pre-annealed cathodes displayed better capacity, cycle performance, rate performance, a much reduced impedance and significant increase of Li-ion diffusion compared to the post-annealed cathode. Following these results, it can be concluded that pre-annealing can be employed to optimise the electrochemical performance of the electrode materials.

Acknowledgements

Author contributions

COE-E conceived, planned, and designed the experiments. KOA and JAA supervised the work. SOA synthesised the cathode materials and performed the electrochemical tests. COE-E wrote the first draft with contributions from SOA. All authors reviewed the manuscript.

Data availability

All data generated or analysed during this study are included in this published article.

Declarations

References

1. A.K. Shukla, Q.M. Ramasse, C. Ophus, D.M. Kepaptsoglou, F.S. Hage, C. Gammer, C. Bowling, P.A.H. Gallegos, S. Venkatachalam, Effect of composition on the structure of lithium and manganese-rich transition metal oxides. Energy Environ. Sci. **11**(4), 830–840 (2018). https://doi.org/10.1039/C7EE02443F

2. F. Wu, N. Li, Y. Su, L. Zhang, L. Bao, J. Wang, L. Chen, Y. Zheng, L. Dai, J. Peng, S. Chen, Ultrathin spinel membrane-encapsulated layered lithium-rich cathode material for advanced Li-ion batteries. Nano Lett. **14**, 3550–3555 (2014). https://doi.org/10.1021/nl501164y

3. B. Xiao, B. Wang, J. Liu, K. Kaliyappan, Q. Sun, Y. Liu, G. Dadheech, M.P. Balogh, L. Yang, T.K. Sham, R. Li, Highly stable $Li_{1.2}Mn_{0.54}Co_{0.13}Ni_{0.13}O_2$ enabled by novel atomic layer deposited AlPO4 coating. Nano Energy **34**, 120–130 (2017). https://doi.org/10.1016/j.nanoen.2017.02.015

4. J. Zheng, X. Wu, Y. Yang, Improved electrochemical performance of $Li[Li_{0.2}Mn_{0.54}Ni_{0.13}Co_{0.13}]O_2$ cathode material

by fluorine incorporation. Electrochim. Acta **105**, 200–208 (2013). https://doi.org/10.1016/j.electacta.2013.04.150

5. D. Liu, X. Fan, Z. Li, T. Liu, M. Sun, C. Qian, M. Ling, Y. Liu, C. Liang, A cation/anion co-doped $Li_{1.12}Na_{0.08}Ni_{0.2-}Mn_{0.6}O_{1.95}F_{0.05}$ cathode for lithium ion batteries. Nano Energy **58**, 786–796 (2019). https://doi.org/10.1016/j.nanoen.2019.01.080

6. C.O. Ehi-Eromosele, S. Indris, N.N. Bramnik, A. Sarapulova, V. Trouillet, L. Pfaffman, G. Melinte, S. Mangold, M.S.D. Darma, M. Knapp, H. Ehrenberg, In situ x-ray diffraction and x-ray absorption spectroscopic studies of a lithium-rich layered positive electrode material: comparison of composite and core–shell structures. ACS Appl. Mater. Interfaces **12**, 13852–13868 (2020). https://doi.org/10.1021/acsami.9b21061

7. J.K. Noh, S. Kim, H. Kim, W. Choi, W. Chang, D. Byun, B.W. Cho, K.Y. Chung, Mechanochemical synthesis of Li_2MnO_3 shell/LiMO2 (M= Ni Co, Mn) core-structured nanocomposites for lithium-ion batteries. Sci. Rep. **4**, 4847 (2014). https://doi.org/10.1038/srep04847

8. J. Yang, F. Cheng, X. Zhang, H. Gao, Z. Tao, J. Chen, Porous $0.2Li_2MnO_3 \cdot 0.8LiNi_{0.5}Mn_{0.5}O_2$ nanorods as cathode materials for lithium-ion batteries. J. Mater. Chem. A **2**, 1636–1640 (2014). https://doi.org/10.1039/C3TA14228K

9. H. He, H. Cong, Y. Sun, L. Zan, Y. Zhang, Spinel-layered integrate structured nanorods with both high capacity and superior high-rate capability as cathode material for lithium-ion batteries. Nano Res. **10**, 556–569 (2017). https://doi.org/10.1007/s12274-016-1314-4

10. N.H. Vu, P. Arunkumar, J.C. Im, D.T. Ngo, H.T.T. Le, C.J. Park, W.B. Im, Effect of synthesis temperature on the structural defects of integrated spinel-layered $Li_{1.2}Mn_{0.75}Ni_{0.25}O_{2+\delta}$: a strategy to develop high-capacity cathode materials for Li-ion batteries. J. Mater. Chem. A **5**, 15730 (2017). https://doi.org/10.1039/C7TA04002D

11. F. Nomura, Y. Liu, T. Tanabe, N. Tamura, T. Tsuda, T. Hagiwara, T. Gunji, T. Ohsaka, F. Matsumoto, Optimization of calcination temperature in preparation of a high capacity Li-rich solid-solution $Li[Li_{0.2}Ni_{0.18}Co_{0.03}Mn_{0.58}]O_2$ material and its cathode performance in lithium ion battery. Electrochim. Acta **269**, 321–330 (2018). https://doi.org/10.1016/j.electacta.2018.03.027

12. C.O. Ehi-Eromosele, S. Indris, G. Melinte, T. Bergfeldt, H. Ehrenberg, Solution combustion-mechanochemical syntheses of composites and core-shell cathode materials for lithium-ion batteries. ACS Sustain. Chem. Eng. **8**, 18590–18605 (2020). https://doi.org/10.1021/acssuschemeng.0c06804

13. M.N. Ates, S. Mukerjee, K.M. Abraham, A high rate Li-rich layered MNC cathode material for lithium-ion batteries. RSC Adv. **5**, 27375–27386 (2015). https://doi.org/10.1039/C4RA17235C

14. J. Li, J. Li, T. Yu, F. Ding, G. Xu, Z. Li, Y. Zhao, F. Kang, Stabilizing the structure and suppressing the voltage decay of Li $[Li_{0.2}Mn_{0.54}Co_{0.13}Ni_{0.13}]O2$ cathode materials for Li-ion batteries via multifunctional Pr oxide surface modification. Ceram. Int. **42**, 18620–18630 (2016). https://doi.org/10.1016/j.ceramint.2016.08.206

15. L. Huang, L. Liu, H. Wu, Y. Wang, H. Liu, Y. Zhang, Optimization of synthesis parameters for uniform sphere-like $Li_{1.2}Mn_{0.54}Ni_{0.13}Co_{0.13}O_2$ as high performance cathode material for lithium ion batteries. J. Alloys Compd. **775**, 921–930 (2019). https://doi.org/10.1016/j.jallcom.2018.10.173

16. S.O. Ajayi, C.O. Ehi-Eromosele, K.O. Ajanaku, Combustion synthesis and characterization of $Li_{1.2}Mn_{0.52}Ni_{0.20}Co_{0.08}O_2$ cathodes for Li-Ion battery: effect of fuel mixture and annealing temperature. Ceram. Int. (2021). https://doi.org/10.1016/j.ceramint.2021.10.009

17. S.B. Waje, M. Hashim, W.D.W. Yussof, Z. Abbas, X-ray Diffraction studies on crystal size evolution of $CoFe_2O_4$ nanoparticles prepared using mechanical alloying and sintering. Appl. Surf. Sci **256**, 3122–3127 (2010). https://doi.org/10.4236/msa.2011.26082

18. Y. Chen, S. Luo, J. Leng, S. Deng, S. Yan, X. Tian, Y. Li, J. Guo, T. Lei, J. Zheng, Exploring the synthesis conditions and formation mechanisms of Li-rich layered oxides via solid-state method. J. Alloys Compd. (2020). https://doi.org/10.1016/j.jallcom.2020.157204

19. R. Suresh, V. Ponnuswamy, R. Mariappan, Effect of annealing temperature on the microstructural, optical and electrical properties of CeO_2 nanoparticles by chemical precipitation method. Appl. Surf. Sci **273**, 457–464 (2013). https://doi.org/10.1016/j.apsusc.2013.02.062

20. C.O. Ehi-Eromosele, S.O. Ajayi, C.N. Onwucha, Optimizing the electrochemical performance of Li_2MnO_3 cathode materials for Li-ion battery using solution combustion synthesis: higher and longer temperature syntheses improves performance. J. Alloys Compd. **861**, 157972 (2021). https://doi.org/10.1016/j.jallcom.2020.157972

21. D. Eum, B. Kim, S.J. Kim, H. Park, J. Wu, S.-P. Cho, G. Yoon, M.H. Lee, S.-K. Jung, W. Yang, W.M. Seong, K. Ku, O. Tamwattana, S.K. Park, I. Hwang, K. Kang, Voltage decay and redox asymmetry mitigation by reversible cation migration in lithium-rich layered oxide electrodes. Nat. Mater. **19**(4), 419–427 (2020). https://doi.org/10.1038/s41563-019-0572-4

22. H.X. Wei, L.B. Tang, Z.Y. Wang, Y.H. Luo, Z.J. He, C. Yan, J. Mao, K. Dai, J.C. Zheng, Comprehensive understanding of

Li/Ni intermixing in layered transition metal oxides. Mater. Today (2021). https://doi.org/10.1016/j.mattod.2021.09.013

23. K.R. Prakasha, A.S. Prakash, A time and energy conserving solution combustion synthesis of nano $Li_{1.2}Ni_{0.13}Mn_{0.54-}Co_{0.13}O_2$ cathode material and its performance in Li-ion batteries. RSC Adv. **5**, 94411–94417 (2015). https://doi.org/10.1039/C5RA19096G

24. Z. Li, H. Zhao, P. Lv, Z. Zhang, Y. Zhang, Z. Du, Y. Teng, L. Zhao, Z. Zhu, Watermelon-like structured SiOx–TiO2@ C Nanocomposite as a high-performance lithium-ion battery anode. Adv. Funct. Mater. **28**(31), 1605711 (2018). https://doi.org/10.1002/adfm.201605711

25. T.F. Yi, X. Han, S.Y. Yang, Y.R. Zhu, Enhanced electro-chemical performance of Li-rich low-Co $Li_{1.2}Mn_{0.56}Ni_{0.16-}Co_{0.08-x}Al_xO_2$ ($0 \leq x \leq 0.08$) as cathode materials. Sci. China

Mater **59**(8), 618–628 (2016). https://doi.org/10.1007/s40843-016-5097-7

26. T.F. Yi, Y.M. Li, S.Y. Yang, Y.R. Zhu, Y. Xie, Improved cycling stability and fast charge–discharge performance of cobalt-free lithium-rich oxides by magnesium-doping. Acs Appl. Mater. Interfaces **8**(47), 32349–32359 (2016). https://doi.org/10.1021/acsami.6b11724

27. Z. Sun, L. Xu, C. Dong, H. Zhang, M. Zhang, Y. Liu, Y. Zhou, Y. Han, Y. Chen, Enhanced cycling stability of boron-doped lithium-rich layered oxide cathode materials by suppressing transition metal migration. J. Mater. Chem. **7**(7), 3375–3383 (2019). https://doi.org/10.1039/C8TA10786F